Journal of Superconductivity and Novel Magnetism (2018) 31:3315–3322
https://doi.org/10.1007/s10948-018-4601-3

ORIGINAL PAPER

Synthesis and Characterization of $NiFe_2O_4$ Nanoparticles for the Enhancement of Direct Sunlight Photocatalytic Degradation of Methyl Orange

Hirthna[1] · S. Sendhilnathan[2] · P. Iyyappa Rajan[3,4] · T. Adinaveen[5]

Received: 18 November 2017 / Accepted: 6 February 2018 / Published online: 17 February 2018

Abstract

The current investigation shows the simple and direct sunlight-mediated photocatalytic degradation of methyl orange dye by quasi globular $NiFe_2O_4$ nanocrystals synthesized from the high-temperature chemical co-precipitation method. The experiment was carried out under direct sunlight which shows significant degradation results lead to the practical possibility of heterogeneous photocatalysis towards environmental remediation. The as-synthesized quasi globular $NiFe_2O_4$ nanocrystals also were characterized by well-known analytical measurements of their structural, morphological, bonding, surface area, band gap and magnetic properties prior to the photocatalytic experiments. The presence of active free radicals formed during the photocatalytic reaction was confirmed from the EPR signals recorded for the solution containing the photocatalyst and dye solution, and accordingly, the photocatalytic degradation mechanism was discussed.

Keywords Quasi globular $NiFe_2O_4$ · Sunlight-mediated synthesis · Photocatalytic degradation · EPR free radical signals

1 Introduction

Heterogeneous photocatalysis has been considered as a promising application towards environmental remediation specifically to dye removal and wastewater treatment [1]. A wide range of investigations has been reported so far in this area using various photocatalysts [2]. However, most studies show the degradation of self-designed photocatalytic reactors [3]. Photocatalytic degradation, an experiment under direct sunlight (a combination of ultraviolet (UV) and visible radiation) with an enhanced efficiency, is currently focused on which can reduce the cost of the equipment, simplify the process and ultimately make a pathway towards bulk-scale reaction. Apart from these perceptions, the choice of the material which can act as an efficient photocatalyst should be given more consideration. In our literature survey [4], we have realized that the magnetically oriented spinel ferrites show excellent catalytic activity towards diversified reactions and extend its applications in numerous fields such as electromagnetic absorbers, sensors, microwave devices, water purification, antibacterial, nanoelectronics, drug delivery and magnetic resonance imaging [5].

The unique structural, electronic, magnetic and optical properties of these materials are the responsible factors of their multiple applications. The magnetic spinel ferrites are generally expressed in the formula AB_2O_4, where A and B are the representation of divalent and trivalent cations [6]. In our present work, we have opted $NiFe_2O_4$, an inverse spinel which has been extensively studied for various applications. For $NiFe_2O_4$ in its inverse spinel structure,

✉ Hirthna
hirthnakumararaja@gmail.com

S. Sendhilnathan
sendhil29@yahoo.co.in

1 Department of Physics, University College of Engineering - Kanchipuram, Kanchipuram, Tamil Nadu 631552, India

2 Department of Physics, University College of Engineering - Pattukottai, Raja madam, Thanjavur, Tamil Nadu 614701, India

3 Chemistry Division, School of Advanced Sciences, Vellore Institute of Technology (VIT) University, Chennai Campus, Vandalur – Kelambakkam Road, Chennai 600127, India

4 Indo-Korea Science and Technology Center, Bengaluru 560064, India

5 Department of Chemistry, Madras Christian College, Chennai 600059, India

Fe^{3+} ions occupy all the tetrahedral sites and half of the octahedral sites, whereas Ni^{2+} occupies the rest of the octahedral sites of the crystal lattice [7]. $NiFe_2O_4$ in nano dimensions exhibit high magnetocrystalline anisotropy and high saturation magnetization with a unique magnetic structure [8]. It possesses a semiconducting band gap of 1.53 eV [9] and so far various methods have been employed to synthesize this material.

The current work utilizes the high-temperature chemical co-precipitation method which is known to be cost-effective, simple handling of reaction, bulk production and high crystalline nature of synthesized nanomaterials [10]. In general, the chemical co-precipitation method was carried out in room temperature, but we believed that the moderately high temperature controlled along with constant stirring has a significant effect on the formation of nanomaterials and hence the reaction temperature was fixed to a moderately high temperature of 100 °C in our synthesis. The synthesized sample was evaluated for its photocatalytic activity on methyl orange dye. The methyl orange dye was considered as an important classification of azo-dye-based environmental pollutant [11]. The adverse effects of this dye can be severe threats to the ecosystem, and the elimination of methyl orange dye was carried out successfully by heterogeneous photocatalytic degradation which was reported in several investigations using various catalysts [12]. However, most of the experiments have been carried out under UV or visible light irradiation in a self-designed photocatalytic reactor [13].

Here, in the current investigation, we are reporting the synthesis of $NiFe_2O_4$ quasi globular nanocrystals and evaluated its photocatalytic activity on methyl orange dye under direct sunlight. This mode of experiments with significant results will lead to the practical possibility of heterogeneous photocatalysis towards environmental remediation. The as-synthesized quasi globular $NiFe_2O_4$ nanocrystals were characterized by the well-known characterization techniques, and the degradation mechanism was also discussed in detail. Also, we promote the utilization of abundantly available solar energy from sunlight, a natural resource for the degradation of dye pollutants in wastewater.

2 Experimental

2.1 Materials

Ferric chloride ($FeCl_3{\cdot}6H_2O$), nickel chloride ($NiCl_2{\cdot}6H_2O$) and sodium hydroxide pellets (NaOH) purchased from Merck Chemicals Ltd., India, were employed for the synthesis of quasi globular $NiFe_2O_4$ nanocrystals without further purification. Double-distilled water was used throughout the experiments.

2.2 Synthesis of Quasi Globular $NiFe_2O_4$ Nanocrystals

A high-temperature chemical co-precipitation method was used in our work for the synthesis of quasi globular $NiFe_2O_4$ nanocrystals. Nickel and ferric chloride salt precursor solutions at the ratio of 1:2 were added to an aqueous solution of 0.5 M sodium hydroxide drop by drop at the temperature of 100 °C under constant stirring for 1 h. This addition results in the conversion of metal hydroxides from their respective salts and immediately transforms into the ferrite formation. A brown-coloured precipitate was obtained which was filtered and washed repeatedly with distilled water to ensure the removal of water-soluble impurities. Finally, the precipitate was dried at 110 °C inside a hot air oven and subjected to calcination in a furnace at 550 °C for 4 h.

2.3 Characterization Methods

An X-ray diffractogram of quasi globular $NiFe_2O_4$ nanocrystals was recorded using a Rigaku Ultima IV high-resolution X-ray diffractometer with Cu Kα radiation at $\lambda = 0.154$ nm. The percentage transmittance of the functional groups present in the sample was measured by using a Perkin Elmer infrared spectrophotometer (model RX l). High-resolution scanning and transmission microscopic analysis (HR-SEM and HR-TEM) with an energy-dispersive X-ray (EDX) spectrum was carried out in a JEOL JSM6360 and JEOL JEM 3010 model electron microscope respectively. Magnetic measurements were carried out at room temperature using the PMC MicroMag3900 model vibrating sample magnetometer (VSM) equipped with a 1-T magnet.

2.4 Photocatalytic Activity Reaction Procedure

Photocatalytic activity of the synthesized quasi globular $NiFe_2O_4$ nanocrystals was analysed using methyl orange dye under direct-solar radiation. To 100 mL of methyl orange dye solution, about 50 mg of catalyst was added. Subsequently, the mixture was stirred in the dark for about 30 min to maintain equilibrium between adsorption and desorption. The resulting suspension was irradiated under direct sunlight at the time interval between 10.30 a.m. to 3.30 p.m. by placing on the top roof of our laboratory, Chennai, India (8°4′ − 37°6′ N latitude) during summer (April–May). The solutions were stirred continuously and open to air environment. The photocatalytic degradation (PCD) efficiency (η) was calculated from the following expression:

$$\eta = \frac{C_i - C_t}{C_i} \times 100 \quad (1)$$

where C_i is the initial concentration of methyl orange and C_t is the concentration of methyl orange after t minutes.

3 Results and Discussion

3.1 Structural Information

X-ray diffraction patterns were recorded for the synthesized quasi globular $NiFe_2O_4$ nanocrystals, and well-defined Bragg's reflections were observed as high-intensity peaks with the absence of any impurity phase. These Bragg's reflections are shown in Fig. 1, and the lattice constant (a_o) was calculated to be 8.27 Å which is in good agreement with the other reported literature [14]. The high-intensity diffraction peaks at 2θ of 30.6, 35.9, 43.7, 57.7 and 63.2 express the high-crystalline nature of quasi globular $NiFe_2O_4$ nanocrystals which corresponded to the reflections of (220), (311), (400), (511) and (440) planes respectively. All the peaks are indexed with the standard JCPDS data with card number 74-2081. A force will be generated during the sintering process, which is the cause of the material density. The uniform grain size distribution is mainly due to the driving force of the homogeneous grain. The strong intensities of (220), (440) and (511) planes are more sensitive towards the cations on octahedral and tetrahedral and the oxygen ion parameters. The B sites will be strongly occupied by Ni^{2+} ions. This shows that the intensities of the planes decline upon the addition of magnesium. The increase in the intensity of the (440) plane is more than that of the (220) plane. The absence of secondary peaks indicates that the as-synthesized quasi globular $NiFe_2O_4$ nanocrystals possess a single-phase cubic structure, and in particular, the high-intensity reflection at the (311) plane significantly denoted the single face-centred cubic spinel phase.

The crystallite size was calculated by the Debye–Scherrer formula using the FWHM value of the respective indexed peak.

$$D = \frac{0.89\lambda}{\beta \cos\theta} \tag{2}$$

where λ is the wavelength of the X-ray radiation ($\lambda = 1.5406$ Å), β is the full width half maximum of the characteristic peak (in radians), θ is the Bragg diffraction angle for the hkl plane and D is the grain size (in nanometres). On the basis of the above formula, the average crystallite size (Dave) of the quasi globular $NiFe_2O_4$ nanocrystals is calculated to be in the range of 16–20 nm in size.

3.2 Bonding Information

The bonding information for the synthesized $NiFe_2O_4$ nanocrystals was analysed through transmittance data obtained from the Fourier transform infrared (FTIR) spectrum in the range of 4000–400 cm^{-1} as shown in Fig. 2. It is very clear that high-frequency bands ($\nu 1$) lie in the range of 580–620 cm^{-1} and 420–435 cm^{-1} ($\nu 2$) corresponds to the lower-frequency bands. These bands confirm the presence of the ferrite group in all the prepared samples. In addition, a broad signal was observed in the range of 3380–3440 cm^{-1} which shows the presence of water symmetric and anti-symmetric stretching. The broadness corresponds to the stretching vibrations of OH groups [17]. The $\nu 1$ and $\nu 2$ bands show the presence of AB_2O_4-type ferrites. The $\nu 3$ band arises due to the presence of divalent metal ion–oxygen complexes on B sites, and the $\nu 4$ band was due to the mass of the divalent tetrahedral cation that appears generally below 400 cm^{-1}, which was not observed in the present study. In addition, bending vibrations of water molecules appeared around ~

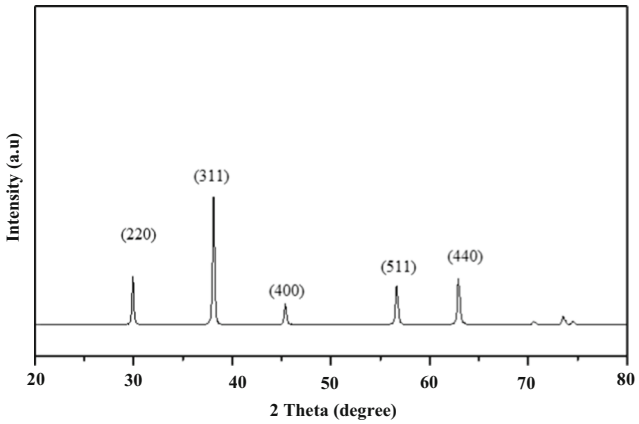

Fig. 1 XRD pattern of $NiFe_2O_4$

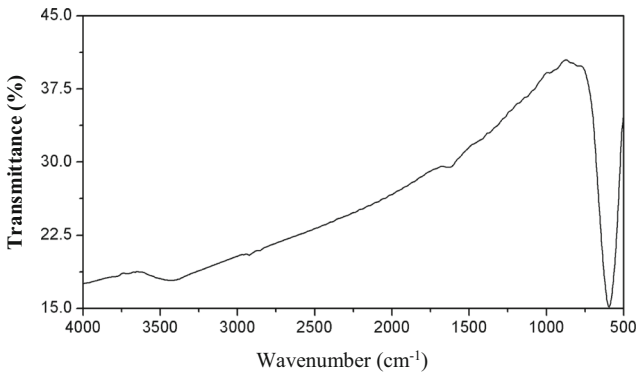

Fig. 2 FT-IR spectra of $NiFe_2O_4$

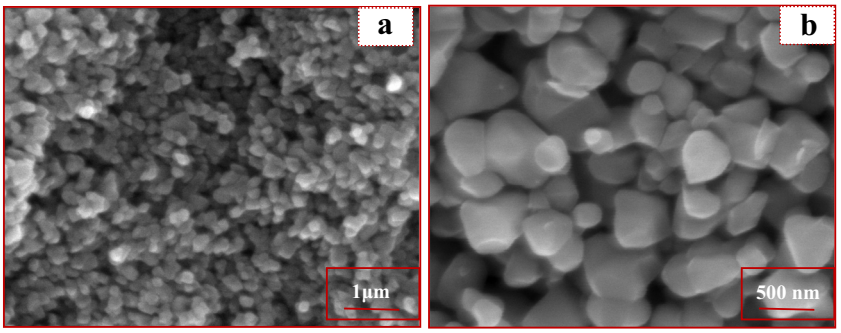

Fig. 3 HR-SEM images of $NiFe_2O_4$. **a** 500 nm, **b** 1 μm

1600 cm^{-1}. The metal–oxygen (Ni–O and Fe–O) intrinsic stretching vibrations in both the octahedral and tetrahedral sites of the crystal lattice are strongly observed in the range 700–400 cm^{-1} [15].

3.3 Morphological, Surface Area and Elemental Composition Information

High-resolution scanning electron microscopic (HR-SEM) images of the synthesized $NiFe_2O_4$ nanocrystals are shown in Fig. 3a, b, and a compact homogeneous arrangement of quasi globular-shaped nanocrystals is clearly visible in the respective micrographs. The particles have no clear boundaries as they aggregate. It is clear from the images that the grain size and boundaries had a great impact on the magnetic, electrical and dielectric properties of these samples. The grain was found to be 25–45 nm, which was measured using the Image-J software associated with the SEM instrument. The irregular arrangement of crystals with high agglomeration may be due to the choice of the synthesis method, existing defects, annealing temperature and the existence of magnetic interactions between the ions in the crystals [16].

Figure 4 shows the elemental composition and purity of the synthesized $NiFe_2O_4$ nanocrystals which confirms both the homogeneity and gradient of the elements Ni, Fe and O present in the sample. The EDX result strongly reveals the single phase formation of the $NiFe_2O_4$ structure from the complete utilization of precursors employed in the synthesis with the absence of other impurities in the samples. The result was in good agreement with the XRD results. Also, the relative atomic ratio of metal ions agrees well with the stoichiometric ratio employed in the synthesis. A small peak around 2.1–2.2 keV is due to the presence of gold, which is employed for the processing of samples in SEM analysis for enhanced morphological visibility. Further in-depth morphological analysis of synthesized $NiFe_2O_4$ nanocrystals was performed on a high-resolution transmission electron microscope (HR-TEM) as displayed in Fig. 5a, b. The HR-TEM images of $NiFe_2O_4$ nanocrystals are self-assembled with high agglomeration, and this could be collectively due to the van der Waals forces and electrostatic interactions between the ions present in the sample [17]. In the current work, a high specific surface area 65.64 m^2/g was obtained for the synthesized $NiFe_2O_4$ nanocrystals. The pore volume was found to be 3.41 cm^3/g.

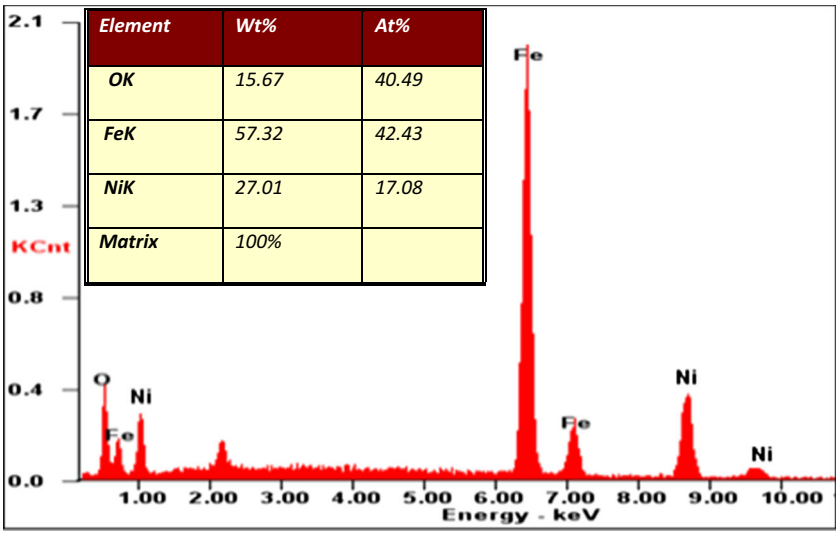

Fig. 4 EDX spectra of $NiFe_2O_4$

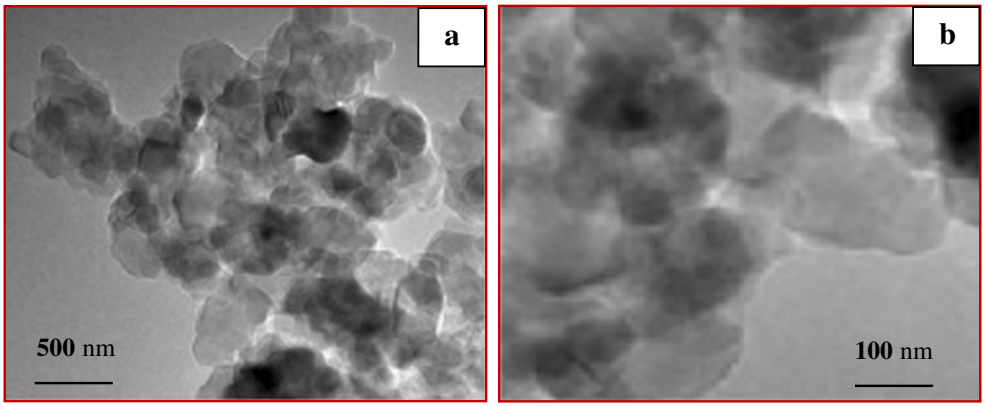

Fig. 5 HR-TEM images of $NiFe_2O_4$. **a** 500 nm, **b** 100 nm

This means that most of the Ni nanoparticles are dispersed on the surface of the ferrite. The corresponding pore size distributions of the nanocatalyst were determined to be 34.74 nm using the Barrett–Joyner–Halenda (BJH) method, indicating that NPs are mesoporous which can be more beneficial for the photocatalytic degradation applications.

3.4 Band Gap Information

To estimate the band gap, the diffuse reflectance spectra (DRS) and photoluminescence spectra of $NiFe_2O_4$ nanocrystals are recorded at room temperature as shown in Fig. 6. A graph was plotted between $[F(R)h\upsilon]^2$ versus $h\upsilon$ by following the modified Kubelka–Munk function [18], and the band gap energy for the $NiFe_2O_4$ nanoparticle is calculated using the formula $E = h\nu = hc/\lambda$. The band gap energy of $NiFe_2O_4$ was found to be in the range between 1.68 and 1.70 eV [19, 20].

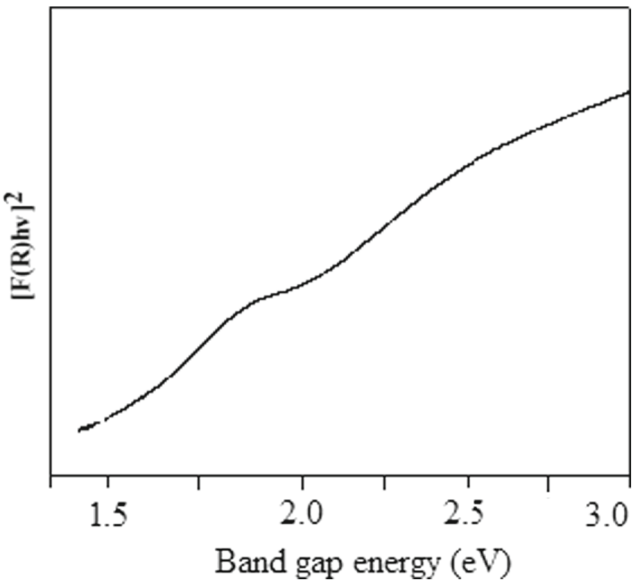

Fig. 6 UV–vis diffuse reflectance spectra of $NiFe_2O_4$

3.5 Magnetic Information

In order to predict the magnetic behaviour of synthesized $NiFe_2O_4$ nanocrystals, the recorded magnetic hysteresis measurements at room temperature are shown in Fig. 7. All the spinel ferrites exhibit hysteresis loops showing the presence of a long-range ferrimagnetic ordering in nickel ferrite nanoparticles. The hysteresis shows that the samples are belonging to a soft ferrite category. The magnetic properties like remanence magnetization (M_r), saturation magnetization (M_s) and coercivity (H_c) were calculated from the hysteresis curves. The saturation magnetization value for bulk nickel ferrite (55 emu/g) is higher than that of the nickel ferrite nanoparticles (38.21 emu/g) [38]. This can be explained based on the spin canting effect and the non-multicollinearity of spin with a magnetic core on the particle surface. The recorded results showed a well-saturated ferromagnetic behaviour with a saturation magnetization (M_s) of 34.91 emu/g and remanent magnetization (M_r) of 0.524 emu/g.

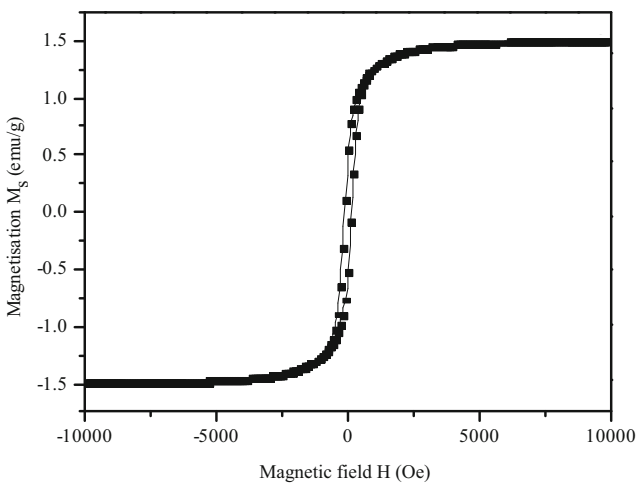

Fig. 7 Magnetic hysteresis (M–H) loops of $NiFe_2O_4$

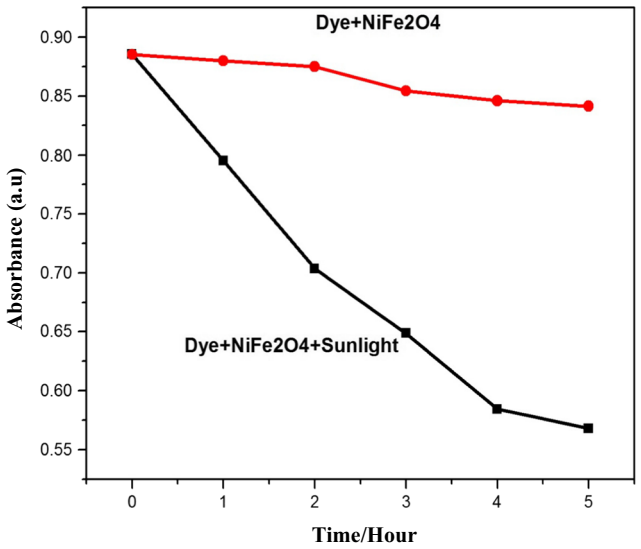

Fig. 8 Plot for absorbance versus time of $NiFe_2O_4$

3.6 Photocatalytic Degradation

Photo catalytic activity experiments were performed for the synthesized $NiFe_2O_4$ nanocrystals on methyl orange dye under direct-solar radiation. The variation in the absorbance of dye molecules is plotted in regular intervals of time as shown in Fig. 8. We have utilized the direct solar radiation from the sunlight which consists of a mixture of UV and visible light, and hence, no wavelength optimization was required in our experiments. Also, we have directed our experiments in neutral pH medium so that the final medium after the degradation can also be expected to be closer to neutral pH; thereby, the final water after degradation can be further used for other purposes.

A known quantity of $NiFe_2O_4$ nanocrystals (200 mg) was fixed as catalyst load, and the concentration of methyl orange dye was taken as 10 mg/L. Our photocatalytic activity experiment results show that there is no significant degradation observed under dark (dye + catalyst only). However, in the presence of $NiFe_2O_4$ nanocrystals, the results show a significant degradation $\sim$ 72.66% of methyl orange dye within 5 h under direct sunlight. This result reveals the high photocatalytic activity of $NiFe_2O_4$ nanocrystals for methyl orange dye degradation.

3.7 Mineralization Analysis

The mineralization process during photocatalytic experiments was carried out with chemical oxygen demand (COD) analysis. The estimated COD of the dye solution before the photocatalytic experiments was estimated to be 6012 mg/L, and after the light illumination, it was significantly reduced to 682 mg/L. The decrease in COD values from 6012 to 682 mg/L confirms the mineralization of methyl orange dye with discolouration. In addition, we have observed in our experiments that the blue colour formed initially during the reaction became faint and finally turned colourless after 5 h.

3.8 Methyl Orange Degradation—EPR Approach

The demonstration of the mechanism of photocatalytic degradation was supported by electron paramagnetic resonance (EPR) signals of solution containing synthesized $NiFe_2O_4$ nanocrystals with the methyl orange dye solution as shown in Fig. 9. In photocatalysis, the electrons are transferred between the reactants and the catalyst; in situ EPR spectroscopy method was used to analyse the electron transfer directly. The value of $g \approx 2.000$ is dissymmetrical

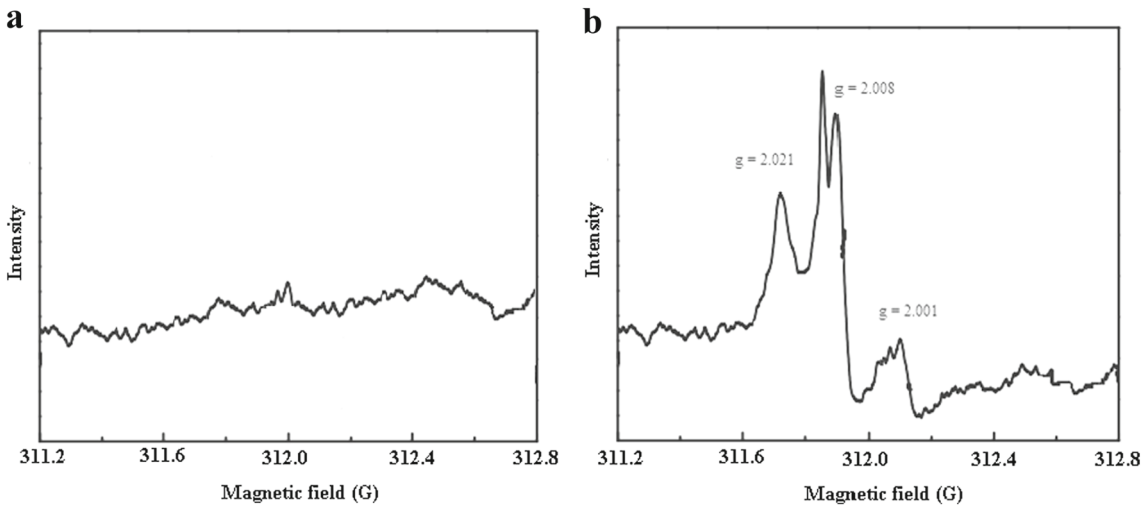

Fig. 9 **a** EPR signals of $NiFe_2O_4$ before illumination and **b** EPR signals of $NiFe_2O_4$ during light illumination

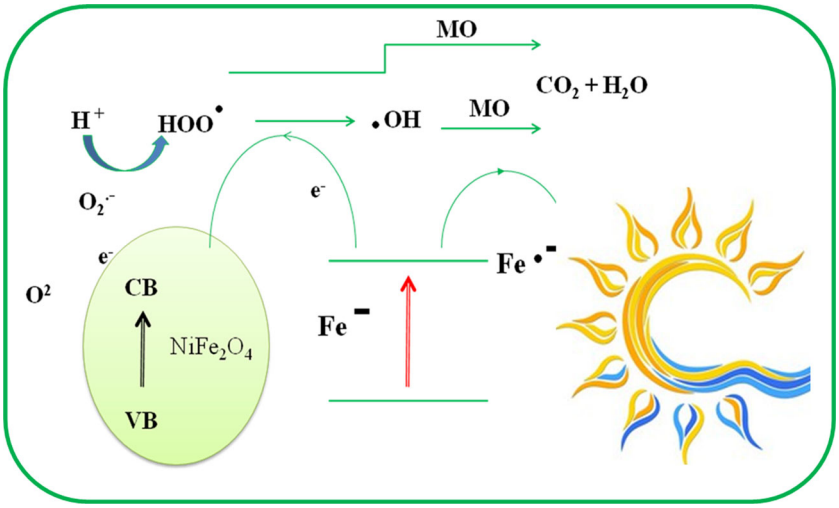

Fig. 10 Photocatalytic degradation reaction mechanism of $NiFe_2O_4$ nanoparticles

with g1 = 2.021 (e^-_{CB} trapped at O vacancies), g2 = 2.008 ($\cdot OH$) and g3 = 2.001 ($\cdot O_2^-$) and confirms the release of a large number of active free radicals which is required to generate reactive species like super oxide radical anion and hydroxide radicals. As well known, the production of these active species will result in effective degradation and, thus, this material plays a major role in enhancing the degradation by effective release of free radicals upon illumination of light. The steps involved in the mechanism of degradation were summarized in the following (3)–(9) and also given as a pictorial representation in Fig. 10.

$$NiFe_2O_4 + h\nu \rightarrow NiFe_2O_4(e^- + h^+) \quad (3)$$

$$NiFe_2O_4(e^-) + O_2 \rightarrow NiFe_2O_4 + {}^{\cdot}O_2^- \quad (4)$$

$$NiFe_2O_4(h^+) + OH^- \rightarrow NiFe_2O_4 + {}^{\cdot}OH \quad (5)$$

$${}^{\cdot}O_2^- + H_2O \text{ molecules} \rightarrow HO_2^{\cdot} + OH^- \quad (6)$$

$${}^{\cdot}OH + \text{pollutants} \rightarrow \text{degradation products} \quad (7)$$

$${}^{\cdot}O_2^- + \text{pollutants} \rightarrow \text{degradation products} \quad (8)$$

$$HO_2^{\cdot} + \text{pollutants} \rightarrow \text{degradation products} \quad (9)$$

Hence, the active free radicals generated from a photocatalytic material have a significant role in degrading the organic pollutants from the wastewater. Similarly, in our results, we have investigated the electron transfer of Fe from the conduction band to the nickel support surface where the electrons are trapped in vacancies in close vicinity of the Ni–Fe_2O_4 interphase. This in situ EPR spectroscopy is the ideal method for studying the electron-transfer process. The formation of active free radicals was confirmed from the EPR signals during the photocatalytic degradation reaction of methyl orange dye by $NiFe_2O_4$ nanocrystals, and hence, this photocatalyst is considered to be a suitable heterogeneous catalyst for the bulk production.

3.9 Estimation of COD

The COD was used to calculate the organic count of the wastewater. The COD of the methyl orange was calculated after and before treatment. The low values in the COD show the mineralization of the dye molecules. The degradation percentage was calculated using the following equation:

$$\text{degradation percentage}\,(\%) = \frac{\text{initial}_{\text{COD}} - \text{final}_{\text{COD}}}{\text{initial}_{\text{COD}}} \times 100 \quad (10)$$

4 Conclusion

The $NiFe_2O_4$ nanocrystals were synthesized using simple high-temperature chemical co-precipitation method which is evaluated for its photocatalytic activity on the degradation of methyl orange dye under direct sunlight through a simple reaction. Our results show that there is no significant degradation observed under the dark condition (dye + catalyst only). However, in the presence of $NiFe_2O_4$ nanocrystals, the results show a significant degradation ~ 72.66% of methyl orange dye solution within 5 h under direct sunlight. This result reveals the high photocatalytic activity of $NiFe_2O_4$ nanocrystals for methyl orange dye degradation. In the mineralization process, the significant decrease in COD values from 6012 to 682 mg/L confirms the mineralization of methyl orange dye with discolouration. The nickel ferrites play a major role in enhancing the degradation by effective release of free radicals upon illumination of light; this was confirmed by the EPR mechanism. Synergy between electron transfer and optical transitions in $NiFe_2O_4$ was visualized by the in situ EPR method.

Acknowledgments Dr. S. Sendhilnathan gratefully acknowledges the DST (Ref. no. SERC no. 100/IFD/7194/2010-11 dated December 10, 2010) for the financial assistance received through the project.

References

1. Nazir, S., Sami, S., Haider, S., Shahid, M., Sher, M., Warsi, M.F., Nadeem, Q., Khan, M.A.: Structural, spectral, dielectric and photocatalytic studies of Zr-Ni doped MnFe2O4 co-precipitated nanoparticles. Ceram. Int. **42**, 13459–13463 (2016)
2. Dong, P., Hou, G., Xi, X., Shao, R., Dong, F.: WO_3-based photocatalysts: morphology control, activity enhancement and multifunctional applications. Environ. Sci.: Nano **4**, 539–557 (2017)
3. Fujishima, A., Honda, K.: Electrochemical photolysis of water at a semiconductor electrode. Nature **238**, 37–38 (1972)
4. Natarajan, K., Bajaj, H.C., Tayade, R.J.: Direct sunlight driven photocatalytic activity of GeO_2/monoclinic-$BiVO_4$ nanoplate composites. Sol. Energ. **148**, 87–97 (2017)
5. Huang, Y., Sudibya, H.G., Chen, P.: Detecting metabolic activities of bacteria using a simple carbon nanotube device for high-throughput screening of anti-bacterial drugs. Biosens. Bioelectron **26**, 4257–4261 (2011)
6. El Moussaoui, H., Mahfoud, T., Habouti, S., El Maalam, K., Ben Ali, M., Hamedoun, M.: Synthesis and magnetic properties of tin spinel ferrites doped manganese. J. Magn. Magn. Mater. **405**, 181–186 (2016)
7. Anandan, S., Selvamani, T., Guru Prasad, G., Asiri, A.M., Wu, J.J.: Magnetic and catalytic properties of inverse spinel $CuFe_2O_4$ nanoparticles. J. Magn. Magn. Mater. **432**, 437–443 (2017)
8. Gautam, S., Shandilya, P., Singh, V.P., Raizada, P., Singh, P.: Solar photocatalytic mineralization of antibiotics using magnetically separable $NiFe_2O_4$ supported onto graphene sand composite and bentonite. J. Water. Process. Eng. **14**, 86–100 (2016)
9. Lazarova, T., Georgieva, M., Tzankov, D., Voykova, D.: Influence of the type of fuel used for the solution combustion synthesis on the structure, morphology and magnetic properties of nanosized $NiFe_2O_4$. J. Alloys Compd. **700**, 272–283 (2017)
10. Peng, Y., Yi, Y., Li, L., Ai, H., Wang, X., Chen, L.: Fe-based soft magnetic composites coated with NiZn ferrite prepared by a co-precipitation method. J. Magn. Magn. Mater. **428**, 148–153 (2017)
11. El Hassani, K., Beakou, B.H., Kalnina, D., Oukani, E., Anouar, A.: Effect of morphological properties of layered double hydroxides on adsorption of azo dye methyl orange: A comparative study. Appl. Clay Sci. **140**, 124–131 (2017)
12. Soltani, T., Lee, B.-K.: Improving heterogeneous photo-Fenton catalytic degradation of toluene under visible light irradiation through Ba-doping in BiFeO3 nanoparticles. J. Mol. Catal. A: Chem. **425**, 199–207 (2016)
13. Peng, Z., Wu, D., Wang, W., Tan, F., Wang, X., Chen, J., Qiao, X.: Effect of metal ion doping on ZnO nanopowders for bacterial inactivation under visible-light irradiation. Powder Technol. **315**, 73–80 (2017)
14. Deraz, N.M., Omar, H.: Abd-Elkader: Preparation and characterization of nanomagnetic Ni-MgFeDeraz, N. M., Omar, H., Abd-Elkader: Preparation and characterization of nanomagnetic Ni-$MgFe_3O_4$ system for biological applications. J. Pure. Appl. Microbio. Microbiology **7**, 333–339 (2013)
15. Deraz, N.M., Omar, H.: Abd-Elakader: Preparation and characterization of nano-magnetic $Ni_{0.5}Mg_{0.5}Fe_2O_4$ system for biological applications. J. Pure Appl. Microbio. **7**, 339 (2013)
16. Selvam, N.C.S., Kumar, R.T., Kennedy, L.J., Vijaya, J.J.: Comparative study of microwave and conventional methods for the preparation and optical properties of novel MgO-micro and nano-structures. J. Alloys Compd. **509**, 9809–9815 (2011)
17. Maa, K., Zhub, J., Xiea, H., Wanga, H.: Effect of porous microstructure on the elastic modulus of plasma-sprayed thermal barrier coatings: experiment and numerical analysis. Surf. Coat. Technol. **235**, 589–595 (2013)
18. Hays, J., Reddy, K.M., Graces, N.Y., Engelhard, M.H., Shutthanandan, V., Luo, M., Xu, C., Giles, N.C., Wang, C., Thevuthasan, S., Punnoose, A.: Effect of Co doping on the structural, optical and magnetic properties of ZnO nanoparticles. J. Phys. Condens. Matter. **19**, 203–206 (2007)
19. Ren, A.O., Liu, C., Hong, Y., Shi, W., Lin, S., Li, P.: Enhanced visible-light-driven photocatalytic activity for antibiotic degradation using magnetic $NiFe_2O_4$/Bi_2O_3 heterostructures. Chem. Eng. J. **258**, 301–308 (2014)
20. Rahmayeni, Z., Novesar Jamarun, E., Arief, S.: Synthesis of ZnO-$NiFe_{2,}O_4$ magnetic nanocomposites by simple solvothermal method for photocatalytic dye degradation under solar light **32**, 1411–1419 (2016). https://doi.org/10.13005/ojc/320315